

Multi-Stage Boundary-Aware Transformer Network for Action Segmentation in Untrimmed Surgical Videos

Rezowan Shuvo^a, M S Mekala^a and Eyad Elyan^a

^aRobert Gordon University, Garthdee House, Aberdeen, AB10 7AQ, United Kingdom

ARTICLE INFO

Keywords:

Surgical workflow analysis
Action segmentation
Boundary detection
Multi-Stage Boundary-Aware Transformer Network (MSBATN)
Hierarchical sliding window attention

ABSTRACT

Understanding actions within surgical workflows is essential for evaluating post-operative outcomes. However, capturing long sequences of actions performed in surgical settings poses challenges, as individual surgeons have their unique approaches shaped by their expertise, leading to significant variability. To tackle this complex problem, we focused on segmentation with precise boundaries, a demanding task due to the inherent variability in action durations and the subtle transitions often observed in untrimmed videos. These transitions, marked by ambiguous starting and ending points, complicate the segmentation process. Traditional models, such as MS-TCN, which depend on large receptive fields, frequently face challenges of over-segmentation (resulting in fragmented segments) or under-segmentation (merging distinct actions). Both of these issues negatively impact the quality of segmentation. To overcome these challenges, we present the Multi-Stage Boundary-Aware Transformer Network (MSBATN) with hierarchical sliding window attention, designed to enhance action segmentation. Our proposed approach incorporates a novel unified loss function that treats action classification and boundary detection as distinct yet interdependent tasks. Unlike traditional binary boundary detection methods, our boundary voting mechanism accurately identifies start and end points by leveraging contextual information. Extensive experiments using three challenging surgical datasets demonstrate the superior performance of the proposed method, achieving state-of-the-art results in F1 scores at thresholds of 25% and 50%, while also delivering comparable performance in other metrics.

1. Introduction

Surgical action segmentation involves analyzing complex elements such as instruments, organs, fluids, or smoke to identify and categorize distinct actions or phases in surgical videos Mascagni, Alapatt, Sestini, Altieri, Madani, Watanabe, Alseidi, Redan, Alfieri, Costamagna et al. (2022). This task is crucial for enhancing surgical training by providing detailed feedback to trainees, improving workflow efficiency and patient safety through real-time monitoring and optimization of procedures, and advancing the performance of autonomous or semi-autonomous surgical robots capable of understanding and executing complex tasks. Recent advancements in this domain have led to the creation of sophisticated architectures tailored to the unique challenges of surgical environments (like Gazebo, ROS2 software development kit (SDK), etc), enabling better decision-making services during operations and driving progress in surgical robotics and education Kiyasseh, Ma, Haque, Miles, Wagner, Donoho, Anandkumar and Hung (2023).

Surgical videos are often heavily annotated manually, where each frame is labelled to a surgical phase or sub-phase or specific action/gesture, as well as the surgical instruments present in that frame Psychogyios, Colleoni, Van Amsterdam, Li, Huang, Li, Jia, Zou, Wang, Liu et al. (2023); Twinanda, Shehata, Mutter, Marescaux, De Mathelin and Padoy (2016). Recent datasets have incorporated action triplets Nwoye, Yu, Gonzalez, Seeliger, Mascagni, Mutter, Marescaux and Padoy (2022), which include action, instrument, and organ information for frame-wise action recognition and instruments or organs segmentation Nwoye, Alapatt, Yu, Vardazaryan, Xia, Zhao, Xia, Jia, Yang, Wang et al. (2023); Chadebecq, Lovat and Stoyanov (2023). However, temporal evolution hierarchies are not well defined as they are subjective in nature. The high to low-level temporal component of a surgical operation or intraoperative activity is termed phase, steps and tasks. For more details please refer attached *supplementary material file*.

Figure 1 demonstrates an effective approach to handle temporal variations by modelling start-end transition in long videos. It starts with frame-wise action and boundary recognition, and then it goes through a segment-wise robust refinement process to avoid over-under segmentation.

 m.shuvo@rgu.ac.uk (R. Shuvo); ms.mekala@rgu.ac.uk (M.S. Mekala); e.elyan@rgu.ac.uk (E. Elyan)
ORCID(s):

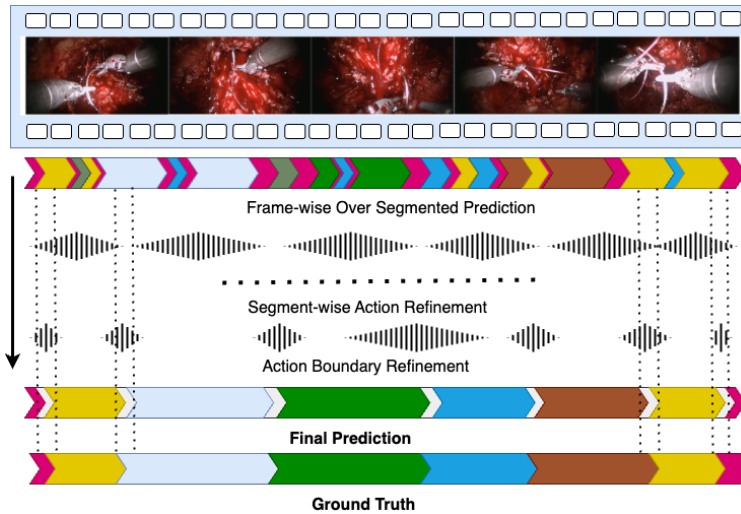


Figure 1: Overview of the proposed framework, which focuses on segments encompassing the action's start, centre, and end, enabling the model to capture nuanced transitions and improve boundary precision.

For efficient analysis of surgical workflows and improving postoperative outcomes, a robust understanding of both spatial context and temporal relationships, the arrangement and transitions between actions or gestures, are essential Chadebecq et al. (2023). In this regard, most publicly available datasets often lack these temporal hierarchies and their evolutions. Additionally, similarities between different phases, including unclear or ambiguous starting, ending and transitions between actions, lead to inaccurate recognition.

For improved surgical video analysis, most existing models are built based on deep neural networks which are broadly divided into single-stage and multi-stage where the architectures evolved from RNN to Temporal Convolution Network (TCN) Farha and Gall (2019); Li, Farha, Liu, Cheng and Gall (2020); Czempiel, Paschali, Keicher, Simson, Feussner, Kim and Navab (2020); Yi, Yang and Jiang (2022), and Transformer Yang, Luo, Wang and Chen (2024); Zhang, Wu and Li (2022); Ding and Li (2022); Nwoye et al. (2022); Shi, Zhong, Cao, Ma, Li and Tao (2023) based approaches. Single-stage models make predictions directly from visual-temporal features. These models utilize a small window of time around the target frame to capture spatial-temporal features, which minimizes computational costs. Early models like EndoNet Twinanda et al. (2016); Twinanda (2017) focused on detecting tool presence and recognizing phases using RNN-based methods. EndoNet Twinanda et al. (2016) is the first method proposed for two tasks simultaneously in a multitasking manner, including tool presence detection and phase recognition. EndoLSTM Twinanda (2017), as the improved EndoNet, replaced hierarchical hidden Markov models (HHMMs) with LSTM for temporal refinement and improved the results substantially. Besides, in Mondal, Sathish and Sheet (2019), a multitask deep learning framework was proposed comprising ResNet-50 and Bi-LSTM. It performs better in tool detection and phase recognition. In Jin, Li, Dou, Chen, Qin, Fu and Heng (2020), a single-staged multitask recurrent convolutional network was proposed with correlation loss (MTRCNet-CL) for surgical video analysis. This multitask learning method used a new correlation loss to minimize tool and phase prediction divergences.

However, RNN and LSTM-based approaches often struggle to capture long-term dependencies that are essential for accurately modelling the entire surgical process. For instance, models like Actionformer Zhang et al. (2022) and Tridet Shi et al. (2023) integrate Transformer architecture for action recognition. However, these single-stage models are designed for small actions while each phase or action segment in surgery takes several minutes, or the whole procedure sometimes takes more than 1 hour. *Because of this research, the single-stage models are not ideal for long untrimmed video analysis.*

Multi-stage models, on the other hand, include an additional refinement stage to improve the initial predictions by correcting the errors. Multi-stage models are considered more suitable for surgical phase recognition to optimize the complexity and ordered nature of surgical activities Czempiel et al. (2020); Van Amsterdam, Funke, Edwards, Speidel, Collins, Sridhar, Kelly, Clarkson and Stoyanov (2022). Multi-stage models such as TeCNOC Czempiel et al. (2020) and Farha and Gall (2019); Li et al. (2020) employ multiple temporal convolutional networks to refine predictions

MSBATN

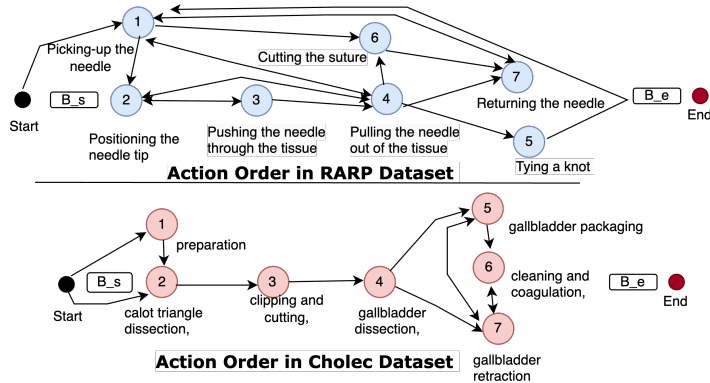


Figure 2: Ambiguous action ordering in untrimmed long surgical videos

in subsequent stages. *However, these methods often neglect high-level semantic information and struggle to refine predictions effectively in an end-to-end manner, leading to over or under-segmentation errors.* This is because the refinement stage focuses on adjusting initial predictions without fully understanding the actions involved during training, and errors remain during inference. This can lead to misinterpretations in complex scenarios where context is crucial. Recently, in Ramesh, Dall’Alba, Gonzalez, Yu, Mascagni, Mutter, Marescaux, Fiorini and Padoy (2021), a multitask multistage temporal convolutional network (MTMS-TCN) was proposed to jointly learn the tasks of phase and step recognition. Some studies applied sensor data with attention mechanism to enhance the understanding of surgical processes Van Amsterdam et al. (2022); Goldbraikh, Shubi, Rubin, Pugh and Laufer (2023), however aligning sensor(kinematic) data with corresponding video frames is complex due to differences in sampling rates and potential time lags(different frequencies), leading to misalignment issues. To improve the segmentation, some research has focused on incorporating segment-level modeling with transformer Ding and Li (2022); Jin, Yu, Chen, Zhao, Heng and Stoyanov (2022). Their main idea is to use high-level segments from surgical videos to clarify ambiguous semantics presented in neighboring frames.

To overcome the above limitations, the current methods use sliding window detectors Czempiel et al. (2020), but they struggle to capture long-term patterns effectively Twinanda et al. (2016); Twinanda (2017); Mondal et al. (2019); Czempiel et al. (2020). Additionally, these approaches overlook the finer details that are essential for understanding the intricate relationships between spatial and temporal features Kiyasseh et al. (2023), resulting in over and under-segmentation errors. The *over-segmentation* occurs when a segment is incorrectly divided into multiple action segments, leading to the detection of more actions than actually exist. These approaches are overly sensitive to minor variations in the input data, causing them to interpret slight changes as new action boundaries Ishikawa, Kasai, Aoki and Kataoka (2021). On the other hand, *Under-segmentation* happens when distinct actions are mistakenly merged into a single segment. *This typically arises due to a lack of sufficient temporal resolution or failure to recognize subtle transitions between different actions.* So, the model overlooks actual action boundaries, resulting in fewer detected action segments than actually exist.

Most of the approaches fail to model the continuous and smooth transitions characteristic of surgical activities due to treating actions and boundaries as discrete events without accounting for their gradual shifts between actions Fard, Ameri, Chinnam and Ellis (2017); Ishikawa et al. (2021). We noticed that the self-attention mechanism has difficulty focusing on important local areas, particularly at the initial layers. Additionally, the encoder-decoder architectures do not effectively refine predictions based on the temporal relationships between actions Yi, Wen and Jiang (2021). To address these issues, first, we propose a framework that extracts spatial features with DinoV2 by discarding irrelevant large patch tokens with register tokens Oquab, Darcet, Moutakanni, Vo, Szafraniec, Khalidov, Fernandez, Haziza, Massa, El-Nouby et al. (2023). Second, for temporal modelling, we present an encoder-decoder model that is built based on the combination of dilated TCN, unified hierarchical and sliding window attention, which captures coarse-to-fine context. The hierarchical representation with dynamic sliding window attention is used to handle long input sequences that organize the attention layers hierarchically to first focus on local relationships and then gradually capture global dependencies. Last, we develop a unified loss function by combining the loss functions of individual tasks into a single

action segmentation to achieve effective boundary detection. This holistic approach allows one to learn multiple tasks simultaneously, leveraging shared representations to improve overall segmentation performance.

Our approach introduces the following key innovations:

- We present a multi-stage TCN-Transformer architecture with dilated acausal convolution to widen the receptive field that predicts and refines both actions and boundaries.
- We introduce hierarchical sliding window attention mechanisms (HSPA) to resolve ambiguities among action orders from different temporal resolution. It links high-level action segment structures with fine-grained frame-wise details, enabling the model to better understand long-term temporal dependencies and immediate frame-level changes.
- We propose a boundary aware loss function that gradually measures cosine similarity from center to boundaries inside action segments that assist in minimizing over or under-segmentation error.

The remainder of this article is structured as follows: Section 2 focuses on related work. Section 3 describes the proposed framework. The model performance is discussed based on experimental evaluation results in Section 4, and the article concludes with Section 5.

2. Related Work

2.1. Action Recognition and Segmentation

For the surgical domain, EndoNetTwinanda et al. (2016) was developed for phase recognition in cholecystectomy videos by learning inherent visual features through a CNN architecture. Recognizing the importance of tool information in phase recognition, EndoNet adopted a multi-task framework that incorporates tool presence detection into the feature learning process. An extension of AlexNet was designed with dual objectives: one part focused on *detecting the presence of surgical tools*, while the other was responsible for *recognizing seven distinct surgical phases*. To capture temporal dependencies, EndoNet integrated a Hierarchical Hidden Markov Model (HMM), enabling the modelling of temporal transitions between phases. The architecture is further improved by LSTMTwinanda (2017) and ResnetTwinanda, Yengera, Mutter, Marescaux and Padoy (2018). However, these methods struggle with accurately identifying transition frames between action phases. To overcome this limitation, a sequence-to-sequence model with an attention mechanism was proposed Namazi, Sankaranarayanan and Devarajan (2019); Yi et al. (2021), which accommodates variable-length inputs and outputs, making it well-suited for detecting overlapping or sequential surgical tasks.

Temporal Action Detection (TAD) methodologies are mainly classified into two-stage and one-stage-based methods. The two-stage approach, inspired by object detection frameworks like Faster R-CNN, involves an initial phase of generating action proposals, followed by subsequent stages of classification and refinement Chao, Vijayanarasimhan, Seybold, Ross, Deng and Sukthankar (2018); Keisham, Jalali and Lee (2022). Although this method often achieves higher accuracy due to its detailed localization process, *it tends to be computationally intensive, posing challenges for real-time applications* Yi et al. (2022). On the other hand, the one-stage approach together consolidates action proposal generation and classification in a single framework, which offers computational efficiency for real-time scenarios. For instance, models like ActionFormer Zhang et al. (2022), and Surgformer Yang et al. (2024) are transformer-based architectures that have achieved enhanced precision of action localization while maintaining computational efficiency. These models capture long-range dependencies and contextual information that helps improve the accuracy of action segmentation and detection. However, *one-stage methods have historically faced difficulties in precisely localizing action boundaries in long untrimmed videos due to their small receptive fields, which is crucial for optimal performance in TAD*.

2.2. Boundary Detection

Identifying action boundaries within untrimmed videos poses unique challenges due to the inherent ambiguity in determining precise start and end points of actions. Initial action boundary detection approaches used probabilistic models to capture temporal dynamics. For example, a spatiotemporal Gaussian Mixture Model (GMM) with Variational Bayesian (VB) Loukas, Nikiteas, Schizas and Georgiou (2016) inference was employed to dynamically estimate the number of components in the GMM, which eliminates the need to predefine the number of clusters. VB inference approximated the full posterior distribution, which improved model flexibility and reduced redundant components.

Table 1
Notation table

Symbol	Description
T	Sequence length (number of frames).
D	Dimensionality of frame features.
\mathbf{x}_t	Feature vector of the t -th frame.
C	Set of action categories (including background).
S	Set of action segments.
W	Base window size for sliding attention.
d	Dilation factor for dilated attention.
T_s	Sequence length at scale s .
α_{ij}^s	Attention weight for token x_i attending to x_j at scale T_s .
$\mathcal{L}_{\text{dice}}$	Dice loss for segment overlap.
\mathcal{L}_{sim}	Gaussian-weighted cosine similarity loss.
$\mathcal{L}_{\text{boundary}}$	Boundary-aware loss for segment precision.
$\alpha, \beta, \gamma, \delta$	Weights for different loss components.
$G(t, t+1)$	Gaussian weight emphasizing temporal proximity.
$G_{\text{boundary}}(t)$	Gaussian weight centered on segment boundaries.

Label assignment and tracking were achieved through Kullback-Leibler (KL) distance, ensuring consistent tracking across video clips. In contrast to rigid boundary detection methods, the Soft-Boundary Unsupervised Gesture Segmentation (Soft-UGS) Fard et al. (2017) approach was proposed as a soft-boundary clustering technique that allowed for gradual transitions between actions. This method utilized kinematic trajectory data, Dynamic Time Warping (DTW), and probabilistic clustering to segment surgical gestures effectively in real-time applications. While these probabilistic models laid the groundwork for more advanced methods, they had limitations in precision, particularly in detecting abrupt transitions in video content.

On the other hand, the advent of deep learning introduced new techniques for addressing the temporal and spatial complexities of action boundary detection. For the surgical domain, sequence models were applied to map variable-length input sequences to output sequences while incorporating attention mechanisms for more accurate boundary localization. A double attention mechanism (such as Namazi et al. (2019)) was introduced to focus specifically on the beginning and end of each surgical phase, offering a refined approach to boundary detection in complex tasks like surgery.

The above methods for temporal segmentation face the issue of over-segmentation because they segment actions into too many sub-components, leading to inaccurate predictions. The Action Segment Refinement Framework (ASRF) Ishikawa et al. (2021) was introduced to address this problem by decoupling frame-wise classification from boundary regression. ASRF refines action segmentation through two branches: one for action predictions and another for boundary regression. By focusing specifically on predicted action boundaries, ASRF achieved overall action localization accuracy. ASRF* Yi et al. (2021) improved the performance with an attention mechanism.

Recent methods, such as TriDet Shi et al. (2023) and Elastic Moment Bounding (EMB) Huang, Jin, Gong and Liu (2022), have further extended the capabilities of one-stage detection for real-time applications. TriDet introduced the Trident-head detection mechanism, which models action boundaries by estimating relative probability distributions instead of directly predicting offsets. *This innovation significantly improved boundary localization accuracy while reducing computational overhead.* EMB tackles uncertainties in temporal boundaries by transforming rigid and manually labelled endpoints into an elastic set of boundaries; however, it does tend to generate a high number of false positives.

Building upon these advancements, our action boundary network employs a voting mechanism to improve segmentation by accurately finding the start and end of an action. By utilizing the predicted action boundaries, our framework refines frame-wise predictions, ultimately improving the performance of action segmentation.

3. Proposed Framework

The action segmentation task involves predicting the action category for each frame in a video. Formally, given a sequence of T -frame features $X = [\mathbf{x}_1, \mathbf{x}_2, \dots, \mathbf{x}_T] \in \mathbb{R}^{T \times d}$, where $\mathbf{x}_t \in \mathbb{R}^d$ represents the d -dimensional feature of the t -th frame. The objective is to predict a sequence of actions $\hat{Y} = [\hat{y}_1, \hat{y}_2, \dots, \hat{y}_T]$, where $\hat{y}_t \in C$. The set

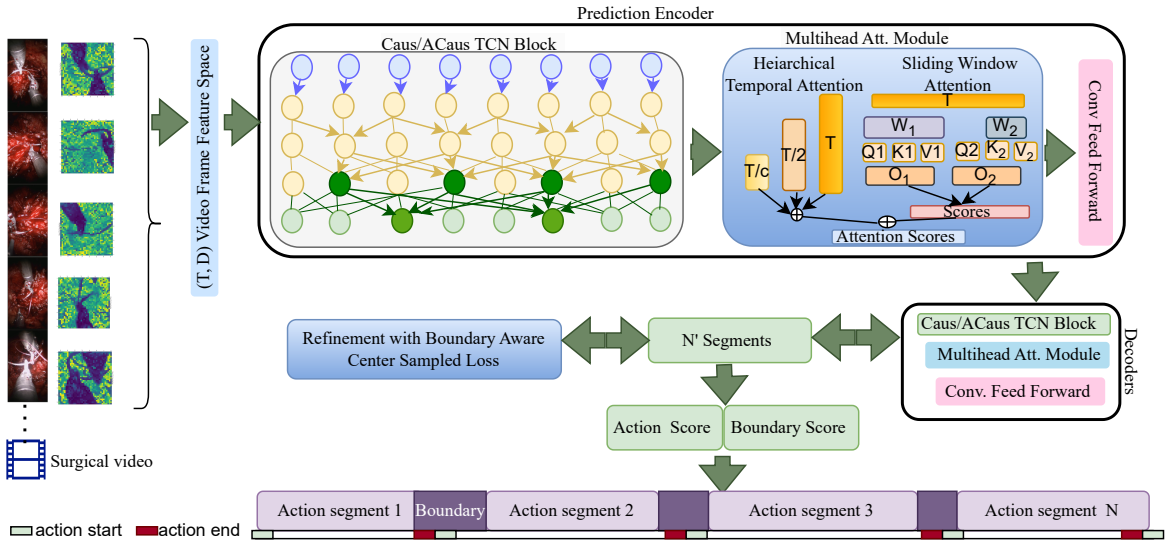


Figure 3: Proposed Multi-Stage Boundary-Aware Transformer Network (MSBATN) architecture

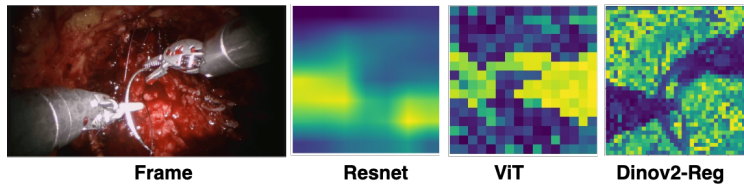


Figure 4: Comparison of frame feature extractors.

$C = \{0, 1, 2, \dots, C, -100\}$ includes all action categories in the dataset, with -100 representing the background class. The frame-wise ground truth labels are $Y = [y_1, y_2, \dots, y_T]$, accompanied by segment information $S = \{(y_{s1}, y_{e1}, a_{c1}), \dots, (y_{sn}, y_{en}, a_{cn})\}$, where y_s and y_e denote the start and end of a segment, a_c represents the action class label, and n is the number of segments, including background segments and notations are listed in Table 1. The goal is to accurately predict action transitions and segment boundaries. Since action transitions are continuous and boundaries are often subjective, considering this 5% of the total segment length is labeled as a transition buffer zone at the start and end of each segment.

Our proposed framework is depicted in figure 3 that enables three distinct parts. First, the frame wise feature extraction, second, Encoder-Decoder architecture with hierarchical sliding window attention, and last, boundary aware loss function that guides to detect the transition with start-center-end points.

3.1. Frame-Wise Feature Extraction

Dino with Register Oquab et al. (2023) (Dinov2-Reg) captures complex spatial features in a self-supervised manner, Figure 4 depicts the performance in comparison with ViT and Resnet. Dinov2-Reg model extracts features using a self-supervised vision transformer model, which processes image-like inputs (frames in this case) to output dense, high-dimensional feature representations. The input feature dimensions (256, 1536), where 256 denotes the 16x16 patch dimension, and 1536 is the feature dimension. A 2D convolutional layer with a kernel size of (256, 1536) is applied to the input frames, which projects the high-dimensional DINO features (256x1536) into a lower-dimensional representation (1x2048). This is equivalent to performing dimensionality reduction via a convolutional operation,

which retains important information while reducing the computational complexity for further processing in a Multi-Stage Boundary-Aware Transformer Network (MSBATN). For more details, please refer to the attached *supplementary material file*.

3.2. Multi-Stage Boundary-Aware Transformer Network (MSBATN)

We present MSBATN transformer-based encoder-decoder architecture without positional encoding to improve the performance of the segmentation task. Each encoder-decoder block comprises a series of TCN and hierarchical sliding window attention modules.

3.2.1. Encoder-Decoder

The frame-wise features (T, D) are passed through an encoder block. The encoder block comprises a series of dilated Acausal Temporal Convolution feed-forward layer blocks to capture context from past and future, followed by the hierarchical sliding window attention module and, lastly, project the encoded features. Instead of using traditional fully connected layers, dilated temporal convolutions are employed to expand the receptive field without increasing the number of parameters or sacrificing resolution. It introduces local inductive biases to effectively capture temporal dependencies and patterns over extended sequences. The model adopts a hierarchical pattern in which the attention layers simultaneously focus on local-global information, mirroring techniques utilized in longformerBeltagy, Peters and Cohan (2020). To capture the global context, we calculated the hierarchical attention at different scales, and then we aggregated to obtain the global context. A detailed discussion is added in the next subsection.

The decoder considered the temporal relationships between action-boundary segments to improve the initial predictions. Similar to the encoder block, the decoder begins with a temporal convolutions block, attention module and output. However, instead of acausal convolution, it has causal convolution, so it does not have any information about the future. Each attention block uses a weighted residual connection to combine the outputs from the feed-forward layers, with the weight α decreasing exponentially across decoders to prevent error accumulation. Last, the decoder generates action boundary labels. The network is comprised of one encoder and three decoders, with each encoder and decoder containing ten TCN-attention blocks. We set the feature dimension in the encoder and decoder layer to 256. Additionally, a temporal dropout layer is applied to the input feature of the encoder, which randomly drops the entire feature channel with a dropout rate of 0.3 to mitigate the over-fitting issue.

3.2.2. Hierarchical dual Sliding Window Attention

Instead of computing attention scores across all token pairs, as in self-attention, we employed a **sparse-attention mechanism**. This approach uses a hierarchical sliding window that restricts attention to a fixed-size window around each token at a specific layer. The window slides and aggregates scores, meaning each token attends only to its neighboring tokens within the specified window. This reduces both space and computational complexity to $O(n)$. To capture temporal dependencies at varying distances, a **dilated attention window** is applied with increasing dilation rates $(0, 1, 2, 3, \dots)$ in each layer. This approach allows for capturing both local details from individual frames and long-term temporal patterns across the sequence. The **action head** and **boundary head** predict the action and start-end labels, respectively Nwoye et al. (2022). For a sequence length T and we define the base temporal window size 64, smallest window size 16, largest window size 512, average number of action segments S . To expand the receptive field, the effective window size W_d for each layer d is calculated using dilation as $W_d = W \cdot (1 + d)$ where W is the base window size, d is the dilation factor ($d = 0, 1, 2, \dots$). For **Dual Window Sliding Attention**, the effective receptive field starts at 16 and grows up to 512, that means $W_d \in [16, 512]$. Local attention is computed within each window and then aggregated across windows. The temporal hierarchical attention operates at multiple scales. The scale T_s is reduced iteratively $T_s = \frac{T}{2^s}$ for $s = 0, 1, 2, \dots$, until $T_s \geq 512$. The average number of scales is approximately $\log_2\left(\frac{T}{S}\right)$, based on the sequence length T and the average number of action segments S . At each scale T_s , **global attention weights** are computed using a sparse mechanism with dilation. For a token x_i attending to token x_j at scale T_s , the attention weight α_{ij}^s is

$$\alpha_{ij}^s = \frac{\exp\left(e_{ij}^s\right)}{\sum_{k \in \mathcal{N}_i^s} \exp\left(e_{ik}^s\right)} \quad (1)$$

where e_{ij}^s is the attention score at scale T_s , \mathcal{N}_i^s is the neighborhood of token x_i at scale T_s , defined by the dilated window size W_d . The final attention is calculated by aggregating scores across all scales and normalizing them with a

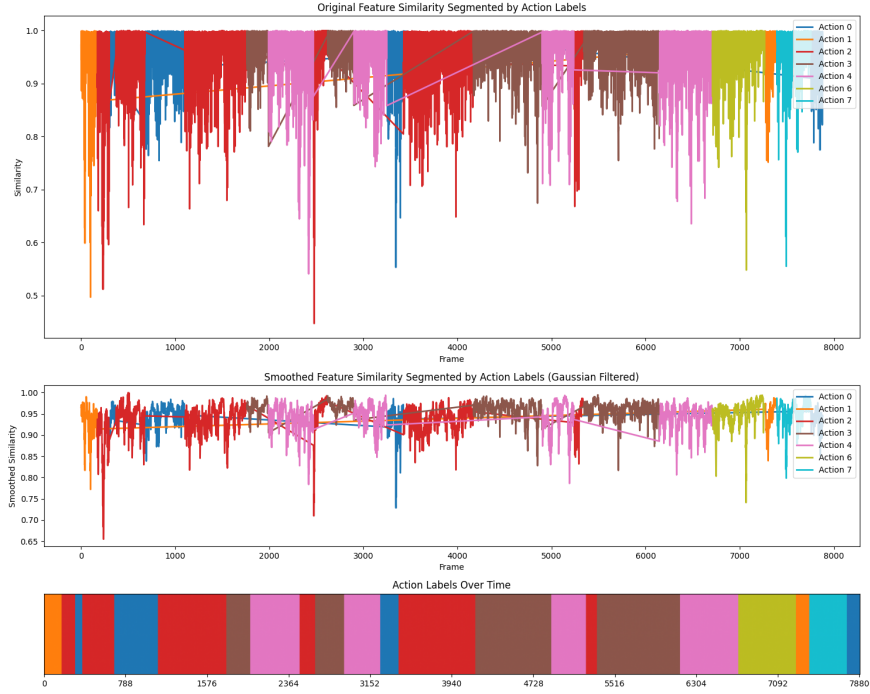


Figure 5: Segment-wise Gaussian-cosine similarity scores for SAR-RARP

softmax function:

$$\alpha_{ij} = \frac{\exp\left(\sum_s e_{ij}^s\right)}{\sum_{k \in \mathcal{N}_i} \exp\left(\sum_s e_{ik}^s\right)} \quad (2)$$

where $\mathcal{N}_i = \bigcup_{s \in S} \mathcal{N}_i^s$ is the union of neighborhoods across all scales, α_{ij} is the final attention weight for token x_i attending to x_j . At each scale T_s , the attention score e_{ij}^s between tokens x_i and x_j within the neighborhood \mathcal{N}_i^s is:

$$e_{ij}^s = \text{sim}(x_i, x_j^s) \quad (3)$$

where x_j^s is the representation of token x_j at scale s , $\text{sim}(\cdot, \cdot)$ is a similarity function (e.g., dot product). By restricting computations to sparse attention neighborhoods \mathcal{N}_i , the computational overhead is significantly reduced while retaining efficiency. The number of scales is determined by $\text{Number of scales} = \log_2\left(\frac{T}{S}\right)$. The scale reduction follows $T_s = \frac{T}{2^s}$, $s = 0, 1, 2, \dots, \log_2\left(\frac{T}{S}\right)$, reducing the sequence length T to approximately $\frac{T}{S}$. For example, if $T = 1000$ and $S = 4$, the segment sizes would be $(1000, 500, 250, 125, \dots)$.

3.3. Boundary-aware Segmentation Loss

In temporal action segmentation, accurately capturing action transitions and segment-level dynamics across varying time scales is crucial. Surgical videos are typically long, and the duration of the segment fluctuates significantly, as shown in Table 2. To address this, we propose a *Boundary-Aware Segmentation Loss* that integrates multiple loss functions, each targeting specific aspects of the segmentation task. To handle class imbalances and ensure precise classification at each timestep, we employ Focal Loss. This loss function down-weights well-classified examples, allowing the model to focus on harder, misclassified examples. This approach is particularly beneficial in datasets where certain action classes are underrepresented. To enhance the overlap between predicted and ground truth segments, we utilize Dice Loss derived from the Dice Coefficient:

$$\text{Dice Coefficient} = \frac{2 \times |A \cap B|}{|A| + |B|} \quad (4)$$

Table 2
Class Duration in SAR-RARP and Cholec80 Datasets

Dataset	ID	Classes/Phases	Mean±Std (s)
SAR-RARP	0	Background Classes	12.4 ± 17.2
	1	Picking-up the needle	3.84 ± 2.66
	2	Positioning the needle tip	6.83 ± 5.65
	3	Pushing needle through tissue	7.51 ± 3.79
	4	Pulling the needle out of tissue	6.77 ± 3.73
	5	Tying a knot	26 ± 7.65
	6	Cutting the suture	6.89 ± 5.31
	7	Returning the needle	6.91 ± 5.41
Cholec80	P1	Preparation	125 ± 95
	P2	Calot triangle dissection	954 ± 538
	P3	Clipping and cutting	168 ± 152
	P4	Gallbladder dissection	857 ± 551
	P5	Gallbladder packaging	98 ± 53
	P6	Cleaning and coagulation	178 ± 166
	P7	Gallbladder retraction	83 ± 56

where A and B represent the predicted and ground truth sets, respectively. The Dice Loss is then formulated as:

$$\mathcal{L}_{\text{dice}} = 1 - \text{Dice Coefficient} \quad (5)$$

This formulation emphasizes the overlap between predictions and ground truth, making it sensitive to both false positives and false negatives. However, focal and dice loss primarily focuses on frame-wise classification accuracy without explicitly considering the temporal relationships between frames. As can be seen in figure 5, the uppermost figure shows the similarity between neighbouring frames, which are ambiguous; we smoothen the distribution by measuring centre-boundary Gaussian weighted cosine similarity depicted in the middle of the figure. To capture temporal dependencies and ensure smooth transitions within action segments, we introduce a loss term based on Gaussian-weighted cosine similarity. This loss penalizes deviations in feature representations between consecutive frames, weighted by a Gaussian function centred on action segments:

$$\mathcal{L}_{\text{sim}} = \sum_{t=1}^{T-1} G(t, t+1) (1 - \cos(\mathbf{f}_t, \mathbf{f}_{t+1})) \quad (6)$$

where $G(t, t+1)$ is the Gaussian weight emphasizing temporal proximity, and $\cos(\mathbf{f}_t, \mathbf{f}_{t+1})$ denotes the cosine similarity between feature vectors at frames t and $t+1$. To further refine boundary precision, we incorporate a Gaussian Similarity Truncated Mean Squared Error (MSE) loss. This loss focuses on boundary regions, applying a Gaussian weight to the MSE, which emphasizes errors near segment boundaries:

$$\mathcal{L}_{\text{boundary}} = \sum_{t=1}^T G_{\text{boundary}}(t) \cdot \min((\hat{b}_t - b_t)^2, \tau) \quad (7)$$

Where $G_{\text{boundary}}(t)$ is a Gaussian weight centred on the boundary, \hat{b}_t and b_t are the predicted and ground truth boundary positions at frame t , and τ is a truncation threshold to limit the influence of large errors. By integrating these loss components, the total temporal loss function is defined as:

$$\mathcal{L}_{\text{temporal}} = \alpha \cdot \mathcal{L}_{\text{class}} + \beta \cdot \mathcal{L}_{\text{dice}} + \gamma \cdot \mathcal{L}_{\text{sim}} + \delta \cdot \mathcal{L}_{\text{boundary}} \quad (8)$$

Where α , β , γ , and δ are weighting factors that balance the contributions of each loss term. This comprehensive loss function enables the model to effectively capture class imbalances, segment overlaps, temporal dependencies, and boundary precision, leading to improved performance in temporal action segmentation tasks.

4. Experiments and Analysis

We extracted every frame (256x 256x3) from the video sequences and used the Dinov2-Reg feature extractor to transform these frames into a 2048-dimensional feature space. These features serve as inputs to our encoder-decoder architecture. The encoder ingests inputs of shape (T, 2048) and processes them through a dilated acausal TCN,

Table 3
Comparison of Models Across Datasets (SAR-RARP, Jigsaw, Cholec80)

Dataset	Settings	Acc	Prec	Rec	F1@10	F1@25	F1@50	Edit
SAR-RARP	CSAtt	0.61	0.68	0.59	0.56	0.52	0.28	0.73
	CHAtt	0.73	0.77	0.71	0.58	0.54	0.40	0.75
	CSFWNO	0.82	0.89	0.80	0.77	0.63	0.49	0.74
	CSSWSO	0.84	0.87	0.82	0.79	0.65	0.51	0.76
	CDWSO	0.87	0.85	0.81	0.85	0.68	0.55	0.79
	CHFW	0.84	0.87	0.81	0.80	0.66	0.52	0.76
	CHDSWO	0.88	0.89	0.80	0.84	0.72	0.58	0.80
	ACSAAtt	0.65	0.67	0.61	0.57	0.57	0.43	0.74
	ACHAtt	0.68	0.65	0.60	0.64	0.60	0.47	0.80
	ACSFWNO	0.87	0.89	0.80	0.83	0.69	0.56	0.79
	ACDWSO	0.88	0.91	0.84	0.84	0.71	0.58	0.81
	ACHFW	0.88	0.90	0.87	0.82	0.71	0.59	0.81
	ACHSSWO	0.89	0.92	0.88	0.85	0.72	0.60	0.82
	ACHDSWO	0.90	0.86	0.87	0.87	0.75	0.64	0.84
Cholec80	CSAtt	0.631	0.712	0.621	0.601	0.585	0.472	0.732
	CHAtt	0.748	0.799	0.728	0.718	0.604	0.503	0.751
	CSFWNO	0.84	0.821	0.83	0.81	0.695	0.583	0.762
	CSSWSO	0.856	0.837	0.846	0.826	0.713	0.604	0.78
	CDWSO	0.89	0.87	0.86	0.86	0.77	0.64	0.84
	CHFW	0.864	0.845	0.854	0.834	0.722	0.614	0.789
	CHDSWO	0.878	0.859	0.868	0.848	0.738	0.631	0.805
	ACSAAtt	0.686	0.767	0.676	0.656	0.547	0.542	0.741
	ACHAtt	0.694	0.754	0.684	0.764	0.656	0.553	0.773
	ACSFWNO	0.89	0.871	0.88	0.86	0.752	0.648	0.819
	ACDWSO	0.902	0.883	0.892	0.872	0.765	0.664	0.832
	ACSSWSO	0.91	0.891	0.9	0.88	0.774	0.675	0.841
	ACHFW	0.906	0.887	0.896	0.876	0.77	0.67	0.837
	ACHDSWO	0.918	0.899	0.908	0.888	0.783	0.686	0.85
Jigsaw	CSAtt	0.742	0.823	0.732	0.712	0.598	0.488	0.705
	CHAtt	0.759	0.84	0.79	0.729	0.617	0.509	0.748
	CSFWNO	0.851	0.832	0.841	0.821	0.708	0.599	0.775
	CSSWSO	0.867	0.848	0.857	0.837	0.726	0.620	0.793
	CDWSO	0.89	0.88	0.887	0.86	0.76	0.638	0.809
	CHFW	0.875	0.856	0.865	0.845	0.735	0.630	0.802
	CHDSWO	0.889	0.87	0.879	0.859	0.751	0.647	0.818
	ACSAAtt	0.797	0.867	0.687	0.867	0.76	0.658	0.827
	ACHAtt	0.905	0.886	0.895	0.875	0.769	0.669	0.836
	ACSFWNO	0.901	0.882	0.891	0.871	0.765	0.664	0.832
	ACDWSO	0.913	0.894	0.903	0.883	0.778	0.680	0.845
	ACHFW	0.917	0.898	0.907	0.887	0.783	0.686	0.85
	ACHFSWO	0.939	0.94	0.929	0.919	0.796	0.723	0.893
	ACHDSWO	0.921	0.902	0.911	0.891	0.787	0.691	0.854

effectively reducing the dimensionality to (T,256) while capturing temporal dependencies over varying scales. These embeddings are further refined through ten layers of multi-head attention mechanisms (with 8 heads), incorporating advanced techniques such as sliding window attention for local dependencies and hierarchical attention for multi-scale temporal modelling. This combination enables the encoder to learn both fine-grained and long-range temporal patterns. The encoder produces frame-level predictions for action classes and boundary classes. To refine these initial predictions, three sequential decoders Zhang, Goel, Sarhan, Goel, Abukhalil, Kalesan, Stottler and Petculescu (2023); Yi et al. (2021); Ishikawa et al. (2021); Yi et al. (2022) are employed. Each decoder shares a similar structure to

Table 4
Comparison with state-of-the-art models Across Datasets (RARP, Cholec80, JIGSAW)

Dataset	Model	Acc	Edit	F1@10	F1@25	F1@50
RARP	MS-TCN Li et al. (2020)	69.0	-	70.7	-	-
	ActionCLIP Psychogyios et al. (2023)	80.4	-	80.6	-	-
	MA-TCN Van Amsterdam et al. (2022)	83.4	81.6	81.7	-	-
	ASRF Ishikawa et al. (2021)	87.5 ± 3.7	83.6 ± 1.9	80.1 ± 3.2	70.8 ± 6.2	59.6 ± 3.2
	NETE Yi et al. (2022)	87.8 ± 3.6	83.9 ± 1.5	78.7 ± 3.6	68.5 ± 3.2	54.6 ± 2.4
	Asformer Yi et al. (2021)	88.8 ± 5.4	84.1 ± 3.1	84.3 ± 5.3	68.1 ± 3.4	59.4 ± 3.1
	MSBATN(Ours)	88.7 ± 3.4	84.3 ± 2.7	84.0 ± 3.7	72.4 ± 2.6	63.8 ± 1.5
Cholec80	ResNet Yi et al. (2022)	78.3	57.8	52.2	-	-
	PhaseLSTM Neil, Pfeiffer and Liu (2016)	80.7	61.2	62.4	-	-
	EndoNet Twinanda et al. (2016)	81.9	-	-	-	-
	TeCNO Czempiel et al. (2020)	88.6	-	-	-	-
	ASRF Ishikawa et al. (2021)	82.5 ± 4.5	78.5 ± 3.5	84.3 ± 3.4	70.6 ± 5.7	60.1 ± 3.4
	Asformer Yi et al. (2021)	82.8 ± 4.7	74.5 ± 6.7	84.1 ± 2.4	70.8 ± 6.2	57.1 ± 3.2
	NETE Yi et al. (2022)	92.8 ± 5.0	78.7 ± 9.4	82.4 ± 3.4	70.1 ± 3.2	53.1 ± 4.8
	MSBATN(Ours)	89.4 ± 2.1	77.5 ± 8.0	84.4 ± 4.4	73.1 ± 5.2	60.2 ± 8.4
JIGSAW	K-TCN Van Amsterdam et al. (2022)	83.8	86.3	90.4	-	-
	MA-TCN Van Amsterdam et al. (2022)	86.8	90.1	93.6	-	-
	ASRF Ishikawa et al. (2021)	87.8 ± 4.5	89.0 ± 2.5	80.4 ± 6.5	70.1 ± 3.6	69.8 ± 2.5
	NETE Yi et al. (2022)	90.8 ± 2.1	86.5 ± 3.5	74.4 ± 7.8	65.1 ± 3.7	58.6 ± 2.9
	Asformer Yi et al. (2021)	92.8 ± 3.3	89.8 ± 6.7	83.5 ± 4.2	70.1 ± 3.5	65.4 ± 1.8
	MSBATN(Ours)	86.1 ± 6.3	89.5 ± 6.5	84.4 ± 5.5	76.1 ± 3.1	70.7 ± 2.8

Table 5
Performance comparison between Start-End Gaussian cosine and BCE Loss

Settings	Start-End Gaussian Cosine Loss				Binary Cross Entropy Loss			
	F1@10	F1@25	F1@50	Edit	F1@10	F1@25	F1@50	Edit (Bin)
ACDWSO	0.85	0.71	0.53	0.81	0.76	0.6	0.58	0.78
ACHFW	0.83	0.7	0.55	0.78	0.7	0.51	0.45	0.72
ACSSWSO	0.86	0.72	0.6	0.82	0.73	0.62	0.55	0.79
ACHDSWO	0.87	0.74	0.63	0.84	0.77	0.64	0.53	0.8

the encoder but focuses on progressively refining predictions with higher accuracy and temporal smoothness. For optimization, we utilized the Adam optimizer along with the softmax activation function to ensure stable training. In contrast to some existing approaches Yi et al. (2021), positional encoding was omitted, as the hierarchical and sliding attention mechanisms sufficiently capture temporal ordering and dependencies. Our boundary-aware loss function is designed to enhance the model’s segmentation and transition detection capabilities. It combines a weighted Dice loss, which penalizes the model based on Intersection over Union (IoU), with a Gaussian Cosine Similarity loss that emphasizes smooth transitions by modelling centre-to-boundary similarity. This composite loss function ensures robust learning of temporal dynamics and accurate identification of action boundaries. We split the dataset into 80-20 ratios for training testing for Jigsaw and Cholec80. We used dropout and early stopping to handle over-fitting and set the max epoch to 120. We have considered three different datasets such as SAR-RARP50Psychogyios et al. (2023), JIGSAWGao, Vedula, Reiley, Ahmidi, Varadarajan, Lin, Tao, Zappella, Béjar, Yuh et al. (2014), Cholec80 Twinanda et al. (2016), and for more details, please refer to supplementary material.

4.1. Evaluation metrics

To evaluate the performance of our models, we used frame-wise accuracy along with segmental-wise overlap. The frame-wise accuracy (FWA) is calculated as $FWA = \frac{\text{correct frames}}{\text{total frames}}$ and to asses the temporal performance, we measured

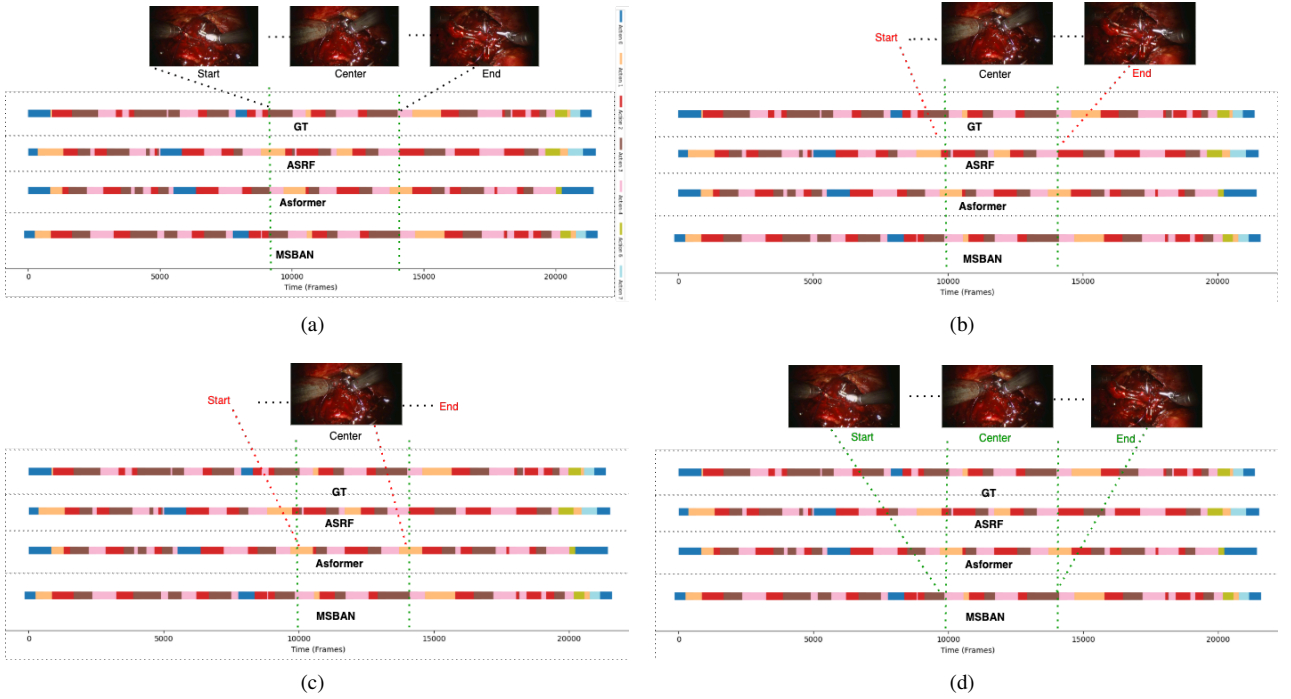


Figure 6: Comparative performance analysis of qualitative segmentation among STOA approaches, where (a) ground truth of actions, (b) ASRF(struggle finding action start), (c) Asformer (struggle finding action start and end), (d) MSBATN (our model)

the segmental scores, which include the segmental edit distance and the segmental F1 score. The Segmental F1 Score measures the temporal overlap between predicted and ground truth action segments. It is computed as the harmonic mean of precision and recall, focusing on how well the predicted segments align with the actual segments in terms of duration and timing. The segmental F1 score was assessed at overlapping thresholds of 10%, 25%, and 50%, referred to as F1@10, F1@25, and F1@50, respectively. Determine True Positives (TP), False Positives (FP), and False Negatives (FN). A predicted segment is considered a TP if its IoU with a ground truth segment exceeds a predefined threshold T . For F1@10%, $T = 0.10$, For F1@25%, $T = 0.25$, For F1@50%, $T = 0.50$. FPs are predicted segments without a matching ground truth segment above the threshold. FNs are ground truth segments without a matching predicted segment above the threshold. Calculate Precision and Recall:

$$\text{Precision} = \frac{\text{TP}_{IoU>T}}{\text{TP}_{IoU>T} + \text{FP}_{IoU>T}}$$

$$\text{Recall} = \frac{\text{TP}_{IoU>T}}{\text{TP}_{IoU>T} + \text{FN}_{IoU>T}}$$

Compute Segmental F1 Score:

$$\text{F1} = 2 \times \frac{\text{Precision} \times \text{Recall}}{\text{Precision} + \text{Recall}}$$

The Edit Score assesses the sequence of predicted action segments by comparing it to the ground truth sequence. It is calculated based on the Levenshtein distance, which quantifies the minimum number of edit operations (insertions, deletions, substitutions) required to transform the predicted sequence into the ground truth sequence. A higher Edit Score indicates a closer match between the predicted and actual sequences, reflecting the model's proficiency in capturing the correct order and transitions of actions. This metric is less sensitive to minor temporal shifts but penalizes over-segmentation and out-of-order predictions. Calculate the Levenshtein distance D between the predicted and

ground truth sequences. The Edit Score is then computed as $\text{Edit Score} = 1 - \frac{D}{\max(L_p, L_g)}$ where L_p and L_g are the lengths of the predicted and ground truth sequences, respectively. The Segmental F1 Score is sensitive to over-segmentation and under-segmentation errors, penalizing models that divide actions into too many segments or fewer segments. In contrast, the Edit Score penalizes incorrect action order and over-segmentation but is more tolerant of slight temporal misalignments. The Segmental F1 Score evaluates the spatial and temporal precision of action boundaries, whereas the Edit Score assesses the structural and sequential accuracy of the predicted action sequence.

4.2. Results Analysis

Our Multi-staged Boundary aware network has three main differences from Asformer, First we employed acausal convolution layer in the initial layers of encoders and decoders. Secondly, we used hierarchical sparse multi-head window attention. Finally, we calculated centre sampled Boundary Aware Loss leverages the strengths of both cosine similarity and Gaussian functions, making it effective for segmentation tasks. We conducted the following experiments to demonstrate the effects of Causal and Acausal convolution along with hierarchical dual or single sliding window attentions.

4.2.1. Effect of Convolution and sliding window attention

We assessed the effectiveness of dilated causal and acausal convolutions, along with various attention settings during training. As illustrated in Table 3, the causal settings include: - Causal Self-Attention (CSAtt) - Causal Hierarchical Attention (CHAtt) - Causal Sliding Fixed Window with No Overlap (CSFWNO) - Causal Sliding Single Window with Overlap (CSSWO) - Causal Dual Sliding Window with Overlap (CDWSO) - Causal Hierarchical Fixed Window with Overlap (CHFOW) - Causal Hierarchical Dual Sliding Window with Overlap (CHDSWO)

In addition, we incorporated acausal convolutions, which include: - Acausal Self-Attention (ACSAtt) - Acausal Hierarchical Attention (ACHAtt) - Acausal Sliding Fixed Window with No Overlap (ACSFWNNO) - Acausal Sliding Single Window with Overlap (ACSSWO) - Acausal Dual Sliding Window with Overlap (ACDWSO) - Acausal Hierarchical Fixed Window with Overlap (ACHFOW) - Acausal Hierarchical Dual Sliding Window with Overlap (ACHDSWO) Through ongoing evaluation of these settings, we concluded that for longer sequences, Dual Sliding Overlapping Window Attention outperformed Single Sliding Overlapping Window. Conversely, for shorter action sequences in the Jigsaw dataset, the Single Sliding Window demonstrated superior performance.

Table 3 highlights the effectiveness of proposed hierarchical sliding window attention with causal and acausal convolution. Settings with acausal convolution performed better than causal convolution as causal convolution restricts information flow to the present and past, ensuring that no future data influences the current output. In contrast, acausal convolution permits the output to depend on past, present, and future input values, which is useful during training. We also observe that self-attention and fixed hierarchical attention performed poorly. Vanilla self-attention computes attention scores between all token pairs, leading to a quadratic complexity. Such complexity becomes prohibitive for long sequences, limiting scalability. Hierarchical attention processes input sequences at multiple hierarchical levels with predetermined structures, which may not adapt well to varying local contexts within the data. Hierarchical Sliding Window Sparse Attention focuses on local neighbourhoods dynamically, capturing essential local patterns and structures. Stacking layers of such windowed attention results in a large receptive field, where top layers have access to all input locations and can build representations that incorporate information across the entire input. Single-Sliding Window Attention performs well on the Jigsaw dataset used in surgical training, where samples are shorter and backgrounds are simpler than in real-world datasets like SAR-RARP and Cholec80. In contrast, Dual-Sliding Window Attention performs better in SAR-RARP and Cholec80, which feature complex and dynamic actions. Single-Sliding Window Attention captures short-range dependencies effectively but may struggle with long-range connections, leading to a fragmented understanding in more complex videos. Meanwhile, Dual-Sliding Window Attention is better at capturing both short- and long-range dependencies, making it suitable for handling diverse action durations and transitions.

4.2.2. Effect of Start-End Boundary Aware Loss Function

Traditional loss functions, such as Binary Cross-Entropy (BCE), predominantly focus on frame-wise classification, which can result in either over-segmentation or under-segmentation. This approach has inherent limitations, particularly when addressing complex or ambiguous boundaries. Additionally, binary boundary classification may lead to instability during training due to substantial variations in loss values both within and between classes. The results of the proposed boundary-aware loss function show that our proposed approach effectively handled these challenges

by capitalizing on the distribution of similarity scores between frames generated by decoders. Table 5 demonstrates the effectiveness of our method, which incorporates actual convolution and sliding window attention settings, delivering improved results across the five metrics outlined in the previous section compared to the binary-boundary-based approach.

5. Conclusion and Feature Work

Segmenting actions in lengthy surgical settings is challenging due to the complex interactions between tools and organs. There are no established standards for optimal performance, as most assessments rely on frame-wise recognition, which has now shifted to segment-wise understanding. In this article, we present a TCN-transformer-based framework with hierarchical sliding window attention that operates with linear computational costs.

We found that selecting the right attention module can be difficult, and neighbouring frames often lead to ambiguous results, causing over- and under-segmentation in frame-wise segmentation. Segment-wise refinement is more effective in improving understanding of surgical activities. Additionally, binary label boundaries are often inadequate because the start, centre, and end of actions vary by individual expertise, leading to poor performance. Our proposed framework addresses these issues with hierarchical sliding window attention for global-local context and includes a novel Boundary Segmentation Loss to better recognize central and boundary points. Our boundary-aware segmentation approach outperforms traditional binary detection methods. Experimental results show that our model matches or exceeds the performance of current state-of-the-art methods across various metrics, ensuring robustness in complex surgical environments.

These results open new interesting research directions, in particular, exploring anticipation tasks where decoders predict the next segment while accounting for uncertainty in a goal-driven manner. Furthermore, integrating instructional prompts to enhance and refine the learning process represents another promising avenue for future investigation.

References

- Beltagy, I., Peters, M.E., Cohan, A., 2020. Longformer: The long-document transformer. arXiv preprint arXiv:2004.05150 .
- Chadebecq, F., Lovat, L.B., Stoyanov, D., 2023. Artificial intelligence and automation in endoscopy and surgery. *Nature Reviews Gastroenterology & Hepatology* 20, 171–182.
- Chao, Y.W., Vijayanarasimhan, S., Seybold, B., Ross, D.A., Deng, J., Sukthankar, R., 2018. Rethinking the faster r-cnn architecture for temporal action localization, in: *Proceedings of the IEEE conference on computer vision and pattern recognition*, pp. 1130–1139.
- Czempiel, T., Paschali, M., Keicher, M., Simson, W., Feussner, H., Kim, S.T., Navab, N., 2020. Tecno: Surgical phase recognition with multi-stage temporal convolutional networks, in: *Medical Image Computing and Computer Assisted Intervention–MICCAI 2020: 23rd International Conference, Lima, Peru, October 4–8, 2020, Proceedings, Part III 23*, Springer. pp. 343–352.
- Ding, X., Li, X., 2022. Exploring segment-level semantics for online phase recognition from surgical videos. *IEEE Transactions on Medical Imaging* 41, 3309–3319. doi:10.1109/TMI.2022.3182995.
- Fard, M.J., Ameri, S., Chinnam, R.B., Ellis, R.D., 2017. Soft boundary approach for unsupervised gesture segmentation in robotic-assisted surgery. *IEEE Robotics and Automation Letters* 2, 171–178. doi:10.1109/LRA.2016.2585303.
- Farha, Y.A., Gall, J., 2019. Ms-tcn: Multi-stage temporal convolutional network for action segmentation, in: *Proceedings of the IEEE/CVF conference on computer vision and pattern recognition*, pp. 3575–3584.
- Gao, Y., Vedula, S.S., Reiley, C.E., Ahmidi, N., Varadarajan, B., Lin, H.C., Tao, L., Zappella, L., Béjar, B., Yuh, D.D., et al., 2014. Jhu-isi gesture and skill assessment working set (jigsaws): A surgical activity dataset for human motion modeling, in: *MICCAI workshop: M2cai*, p. 3.
- Goldbraikh, A., Shubi, O., Rubin, O., Pugh, C.M., Laufer, S., 2023. Kinematic data-based action segmentation for surgical applications. arXiv preprint arXiv:2303.07814 .
- Huang, J., Jin, H., Gong, S., Liu, Y., 2022. Video activity localisation with uncertainties in temporal boundary, in: *European Conference on Computer Vision*, Springer. pp. 724–740.
- Ishikawa, Y., Kasai, S., Aoki, Y., Kataoka, H., 2021. Alleviating over-segmentation errors by detecting action boundaries, in: *Proceedings of the IEEE/CVF winter conference on applications of computer vision*, pp. 2322–2331.
- Jin, Y., Li, H., Dou, Q., Chen, H., Qin, J., Fu, C.W., Heng, P.A., 2020. Multi-task recurrent convolutional network with correlation loss for surgical video analysis. *Medical image analysis* 59, 101572.
- Jin, Y., Yu, Y., Chen, C., Zhao, Z., Heng, P.A., Stoyanov, D., 2022. Exploring intra-and inter-video relation for surgical semantic scene segmentation. *IEEE Transactions on Medical Imaging* 41, 2991–3002.
- Keisham, K., Jalali, A., Lee, M., 2022. Online action proposal generation using spatio-temporal attention network. *Neural Networks* 153, 518–529.
- Kiyasseh, D., Ma, R., Haque, T.F., Miles, B.J., Wagner, C., Donoho, D.A., Anandkumar, A., Hung, A.J., 2023. A vision transformer for decoding surgeon activity from surgical videos. *Nature biomedical engineering* 7, 780–796.
- Li, S., Farha, Y.A., Liu, Y., Cheng, M.M., Gall, J., 2020. Ms-tcn++: Multi-stage temporal convolutional network for action segmentation. *IEEE transactions on pattern analysis and machine intelligence* 45, 6647–6658.
- Loukas, C., Nikiteas, N., Schizas, D., Georgiou, E., 2016. Shot boundary detection in endoscopic surgery videos using a variational bayesian framework. *International journal of computer assisted radiology and surgery* 11, 1937–1949.

- Mascagni, P., Alapatt, D., Sestini, L., Altieri, M.S., Madani, A., Watanabe, Y., Alseidi, A., Redan, J.A., Alfieri, S., Costamagna, G., et al., 2022. Computer vision in surgery: from potential to clinical value. *npj Digital Medicine* 5, 163.
- Mondal, S.S., Sathish, R., Sheet, D., 2019. Multitask learning of temporal connectionism in convolutional networks using a joint distribution loss function to simultaneously identify tools and phase in surgical videos. *arXiv preprint arXiv:1905.08315*.
- Namazi, B., Sankaranarayanan, G., Devarajan, V., 2019. Attention-based surgical phase boundaries detection in laparoscopic videos, in: 2019 International Conference on Computational Science and Computational Intelligence (CSCI), pp. 577–583. doi:10.1109/CSCI49370.2019.00109.
- Neil, D., Pfeiffer, M., Liu, S.C., 2016. Phased lstm: Accelerating recurrent network training for long or event-based sequences. *Advances in neural information processing systems* 29.
- Nwoye, C.I., Alapatt, D., Yu, T., Vardazaryan, A., Xia, F., Zhao, Z., Xia, T., Jia, F., Yang, Y., Wang, H., et al., 2023. Cholectriplet2021: A benchmark challenge for surgical action triplet recognition. *Medical Image Analysis* 86, 102803.
- Nwoye, C.I., Yu, T., Gonzalez, C., Seeliger, B., Mascagni, P., Mutter, D., Marescaux, J., Padoy, N., 2022. Rendezvous: Attention mechanisms for the recognition of surgical action triplets in endoscopic videos. *Medical Image Analysis* 78, 102433.
- Oquab, M., Darcet, T., Moutakanni, T., Vo, H., Szafraniec, M., Khalidov, V., Fernandez, P., Haziza, D., Massa, F., El-Nouby, A., et al., 2023. Dinov2: Learning robust visual features without supervision. *arXiv preprint arXiv:2304.07193*.
- Psychogyios, D., Colleoni, E., Van Amsterdam, B., Li, C.Y., Huang, S.Y., Li, Y., Jia, F., Zou, B., Wang, G., Liu, Y., et al., 2023. Sarrap50: Segmentation of surgical instrumentation and action recognition on robot-assisted radical prostatectomy challenge. *arXiv preprint arXiv:2401.00496*.
- Ramesh, S., Dall’Alba, D., Gonzalez, C., Yu, T., Mascagni, P., Mutter, D., Marescaux, J., Fiorini, P., Padoy, N., 2021. Multi-task temporal convolutional networks for joint recognition of surgical phases and steps in gastric bypass procedures. *International journal of computer assisted radiology and surgery* 16, 1111–1119.
- Shi, D., Zhong, Y., Cao, Q., Ma, L., Li, J., Tao, D., 2023. Tridet: Temporal action detection with relative boundary modeling, in: *Proceedings of the IEEE/CVF Conference on Computer Vision and Pattern Recognition*, pp. 18857–18866.
- Twinanda, A.P., 2017. Vision-based approaches for surgical activity recognition using laparoscopic and RGBD videos. Ph.D. thesis. Strasbourg.
- Twinanda, A.P., Shehata, S., Mutter, D., Marescaux, J., De Mathelin, M., Padoy, N., 2016. Endonet: a deep architecture for recognition tasks on laparoscopic videos. *IEEE transactions on medical imaging* 36, 86–97.
- Twinanda, A.P., Yengera, G., Mutter, D., Marescaux, J., Padoy, N., 2018. Rsdnet: Learning to predict remaining surgery duration from laparoscopic videos without manual annotations. *IEEE transactions on medical imaging* 38, 1069–1078.
- Van Amsterdam, B., Funke, I., Edwards, E., Speidel, S., Collins, J., Sridhar, A., Kelly, J., Clarkson, M.J., Stoyanov, D., 2022. Gesture recognition in robotic surgery with multimodal attention. *IEEE Transactions on Medical Imaging* 41, 1677–1687.
- Yang, S., Luo, L., Wang, Q., Chen, H., 2024. Surgformer: Surgical transformer with hierarchical temporal attention for surgical phase recognition. *arXiv preprint arXiv:2408.03867*.
- Yi, F., Wen, H., Jiang, T., 2021. Asformer: Transformer for action segmentation. *arXiv preprint arXiv:2110.08568*.
- Yi, F., Yang, Y., Jiang, T., 2022. Not end-to-end: Explore multi-stage architecture for online surgical phase recognition, in: *Proceedings of the Asian Conference on Computer Vision*, pp. 2613–2628.
- Zhang, B., Goel, B., Sarhan, M.H., Goel, V.K., Abukhalil, R., Kalesan, B., Stottler, N., Petculescu, S., 2023. Surgical workflow recognition with temporal convolution and transformer for action segmentation. *International Journal of Computer Assisted Radiology and Surgery* 18, 785–794.
- Zhang, C.L., Wu, J., Li, Y., 2022. Actionformer: Localizing moments of actions with transformers, in: *European Conference on Computer Vision*, Springer. pp. 492–510.